

## Electronic Supplementary Information

### **Tissue-Derived Carbon Microbelt Paper: A High-Initial-Coulombic-Efficiency and Low-Discharge-Platform K<sup>+</sup>-Storage Anode for 4.5 V Hybrid Capacitors**

Taoqiu Zhang, Zhiefei Mao, Xiaojun Shi, Jun Jin, Beibei He, Rui Wang, Yansheng Gong, Huanwen

Wang\*

*Engineering Research Center of Nano-Geomaterials of Ministry of Education, Faculty of Material  
and Chemistry, China University of Geosciences, Wuhan, 430074, China.*

E-mail: [wanghw@cug.edu.cn](mailto:wanghw@cug.edu.cn)

**Materials and Reagents:** The tissue was taken from those most commonly used in the laboratory and in everyday life, furthermore, no reagents were used in the material synthesis part of this work.

**Preparation of HCMBs:** The tissue was first heated in air at a heating rate of  $0.5\text{ }^{\circ}\text{C min}^{-1}$  at  $250\text{ }^{\circ}\text{C}$  for 1 h. When the furnace was cooled to room temperature, a pre-oxidation carbonaceous microbelt paper (abbreviated as POCMB) was obtained. This POCMB was then further annealed in argon at 700, 900, 1100 or  $1300\text{ }^{\circ}\text{C}$  for 3 h at a heating rate of  $3\text{ }^{\circ}\text{C min}^{-1}$ . After natural cooling to room temperature, the HCMB-X (X represents the carbonization temperature) could be collected.

**Materials Characterization:** The microstructure was measured by XRD (Bruker AXS D8-Focus, Cu), X-ray photoelectron spectroscopy (XPS, VG Multilab2000), scanning electron microscopy (SEM, Hitachi SU3500), Raman microscope (Renishaw RM-1000, 532 nm excitation) and transmission electron microscopy (TEM, Philips CM12 TEM/STEM).

**Electrochemical characterizations:** The electrochemical characterizations were carried out in CR2032-type coin cells. All the half-cells were constructed with Potassium metal as the counter electrode. The flexible HCMB papers were directly used as the working electrodes. The HCMBs film was cut into  $0.6\text{ cm} \times 0.6\text{ cm}$  size for direct use as anode. The mass loading of HCMB-1300 is determined to be about  $1.5\text{ mg cm}^{-2}$ . The AC electrode was prepared by mixing the active material (80 wt%), acetylene black (10 wt%), and polyvinylidene difluoride (PVDF) (10 wt%) in N-methyl pyrrolidone (NMP), and then the as-obtained slurry was casted on Al foil. Afterwards, the electrodes were dried under vacuum at  $80\text{ }^{\circ}\text{C}$  for 12 h.  $0.8\text{ M KPF}_6$  in ethylene carbonate/dimethyl carbonate (EC/DMC, volume ratio of EC/DMC = 1:1) acted as the electrolyte. For the powdered HCMB material, the working electrodes were prepared by first mixing 80wt% HCMBs powder (obtained by grinding the HCMB paper), 10 wt% super P and 10 wt% PVDF in NMP. The slurry was casted on the Al foil and then dried under vacuum at  $80^{\circ}\text{C}$  for 12 hours. Cyclic voltammogram (CV) profiles were measured in a potential window of 0.01-3.0 V vs.  $\text{K}^+/\text{K}$  on a CHI 750E electrochemical workstation.

Galvanostatic charge–discharge measurements in the range 0.01–3.0 V were performed on the LAND-CT2001A battery test system. The electrochemical intermittent titration technique (GITT) tests were carried out under constant current conditions for 1/3 hour at 0.1 A g<sup>-1</sup> with a relaxation time of 8 hours per charge/discharge.

The HCMB//AC PIC device was fabricated using HCMB-1300 as the anode and AC as the cathode. HCMBs film-1300 was pre-activated for 5 cycles at 0.1 A g<sup>-1</sup> for pre-potassiation to fabrication of the full PIC cell. Activated HCMB-1300 anodes and the AC cathodes were then used for the PIC assembly. The mass ratio of anode to cathode was controlled to be around 1:2.5 to 1:3. The sepiolite/PVDF-(HFP) membrane was prepared according to our previous works (Adv. Energy Mater. 2018, 8, 1702769; Small 2019, 15, 1902466). Specifically, P(VDF-HFP) powder (0.7 g) and sepiolite (0.1 g) was dissolved in 8 g DMF at 80 °C. The solution was coated on a glass substrate and then exposed to water vapor. The obtained sepiolite/PVDF-(HFP) membrane was dried under vacuum. Finally, the above membranes were immersed in 0.8 M KPF<sub>6</sub> in EC:DEC=1:1 in a glove box for 24 hours. The application of this hybrid polymer electrolyte can improve the safety of the PICs compared to the liquid electrolyte.

The energy density and power density are calculated by using equations:  $P = \Delta E/m$  and  $E = Pt$ , where  $\Delta E = (E_{max} + E_{min})/2$ ,  $V_{max}$  and  $V_{min}$  are the beginning and end of the potential in the discharge curve,  $I$  is the charge-discharge current (A),  $t$  is the discharge time (h), and  $m$  is the mass of the active material, including both anode and cathode.

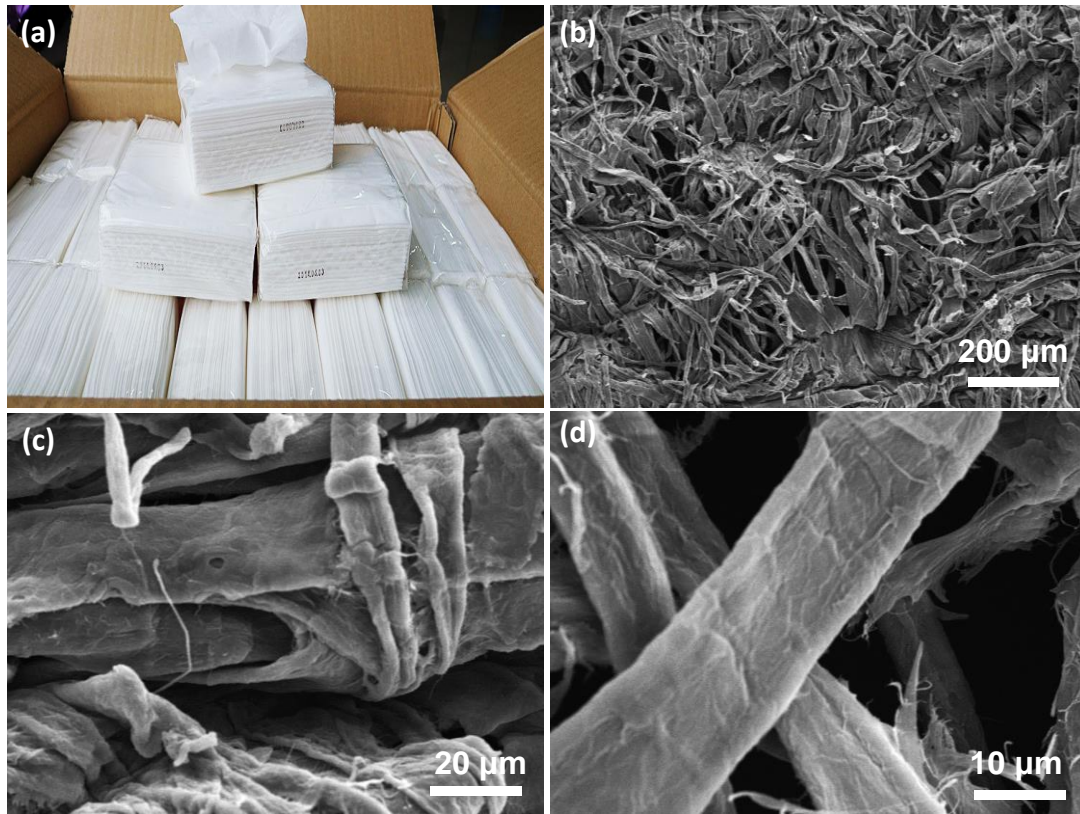


**Fig. S1** (a) Photographs of the tissue precursor, (b, c and d) SEM images of the tissue precursor.

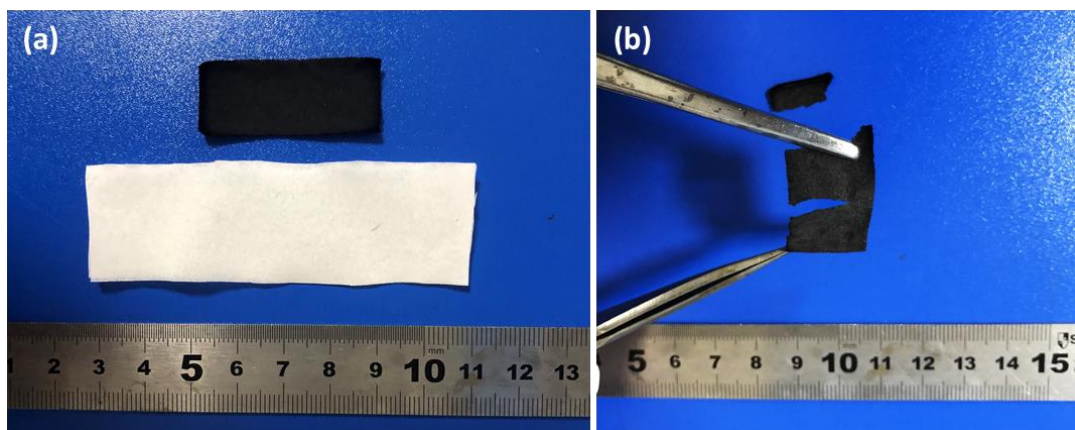


**Fig. S2** Photographs of HCMB-1300 without pre-oxidation.

The pre-oxidation can guarantee strong mechanical flexibility, which is usually observed in polyacrylonitrile-derived carbon nanofiber membranes. If there is no pre-oxidation, the area of the tissue shrinks to about 1/4 of its original size after carbonization at 1300 °C (Fig. S3a). Moreover, the HCMB-1300 without pre-oxidation becomes fragile (Fig. S3b). If the tissue has undergone this step of pre-oxidation, its shrinkage in area can be ignored because pre-oxidation can remove some lignin, natural tar and other substances from the raw material.

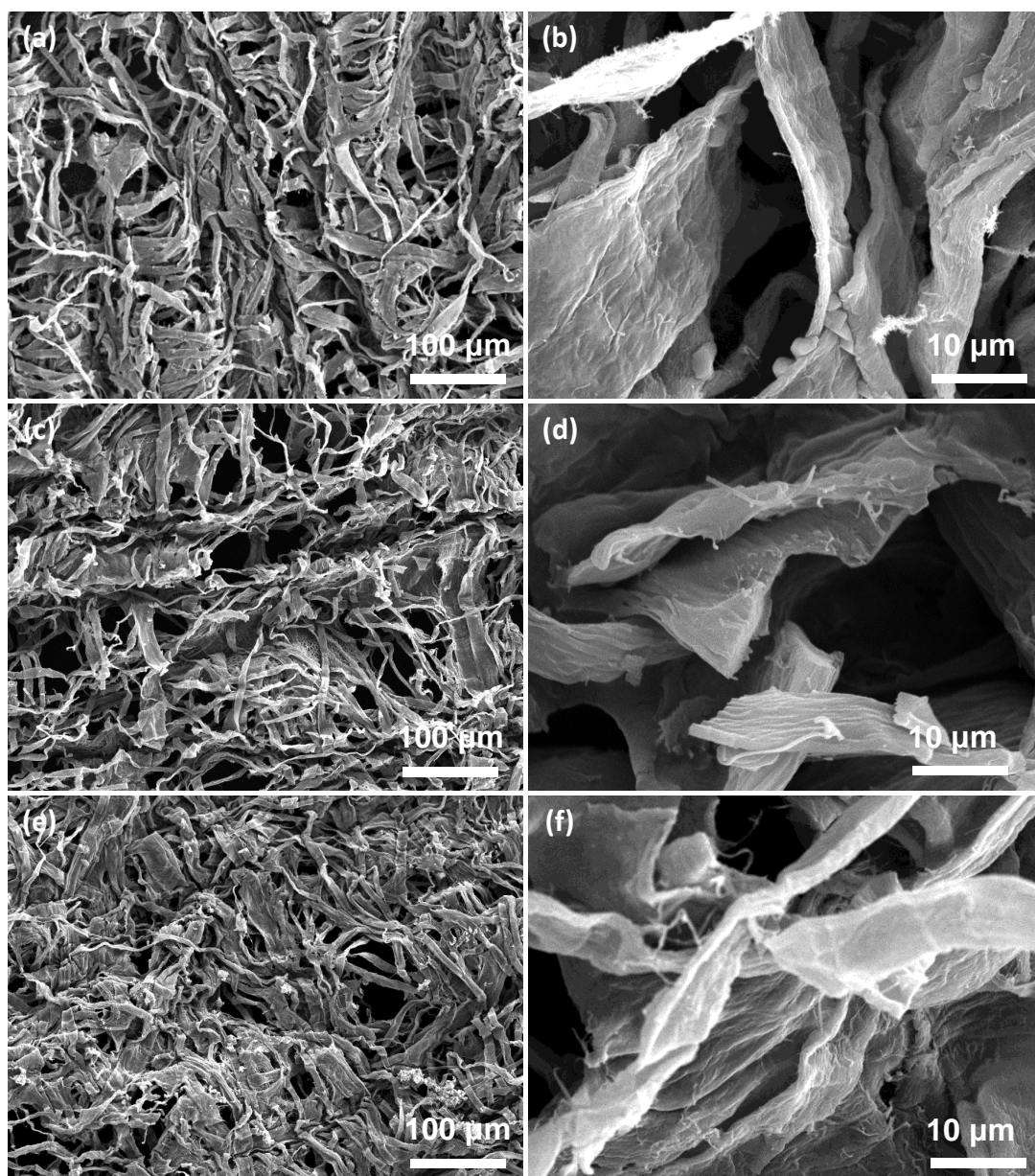


**Fig. S3** SEM images of (a,b) HCMB-700, (c,d) HCMB-900, (e,f) HCMB-1100.

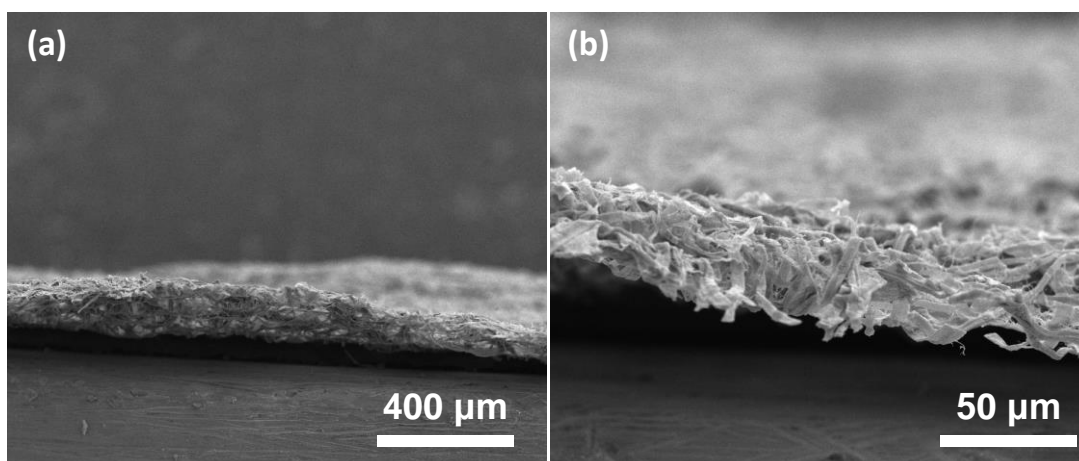


**Fig. S4** Cross-section SEM images of HCMB-1300.

Sample	D peaks (cm <sup>-1</sup> )	G peaks (cm <sup>-1</sup> )	I <sub>D</sub> /I <sub>G</sub>
HCMB-700	1336.91	1604.76	0.91
HCMB-900	1354.76	1603.96	1.02
HCMB-1100	1344.43	1590.55	1.04
HCMB-1300	1339.1	1598.06	1.07

**Table S1.** The wavenumber of the D and G peaks and I<sub>D</sub>/I<sub>G</sub> ratios for samples at different temperatures.

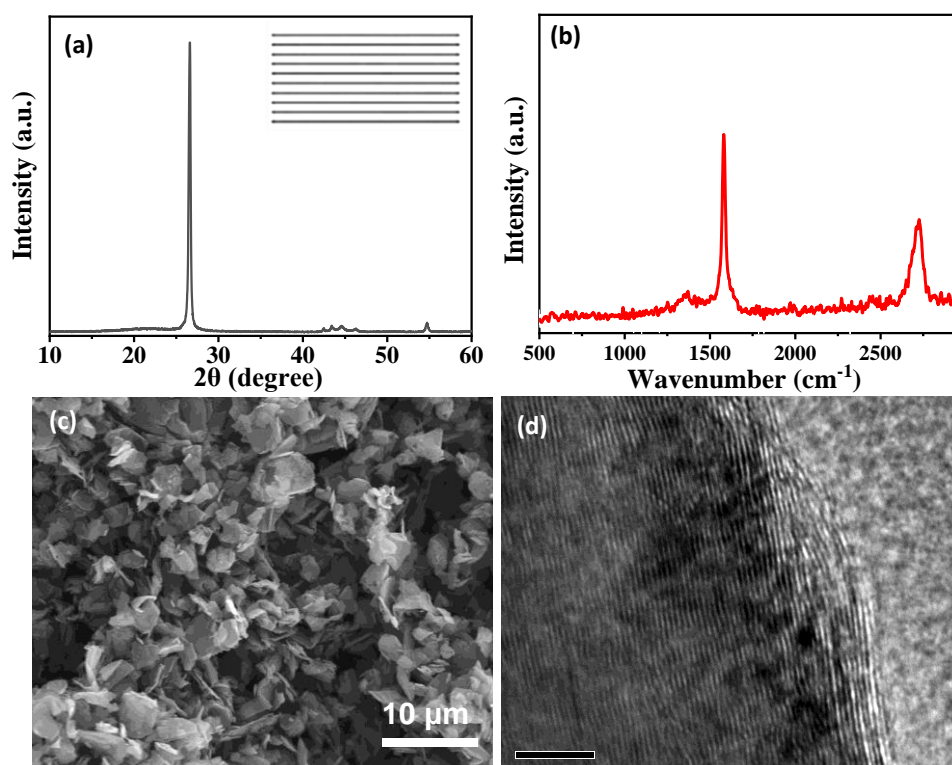


**Fig. S5** Structure and morphology of graphite. (a) XRD patterns, the inset shows a schematic diagram of the graphite structure, (b) Raman spectra, (c) SEM images, (d) TEM images.

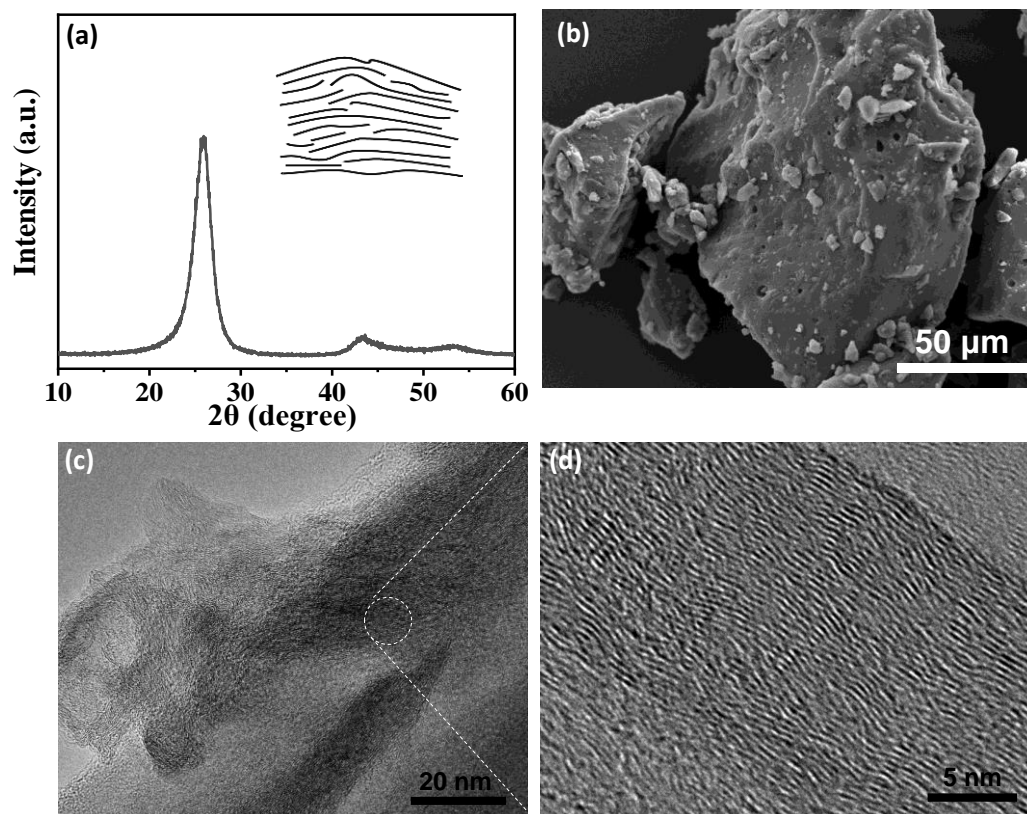


**Fig. S6** Structure and morphology of pitch-derived soft carbon. (a) XRD patterns, the inset shows a schematic diagram of the soft carbon structure, (b) SEM images, (c, d) TEM images.

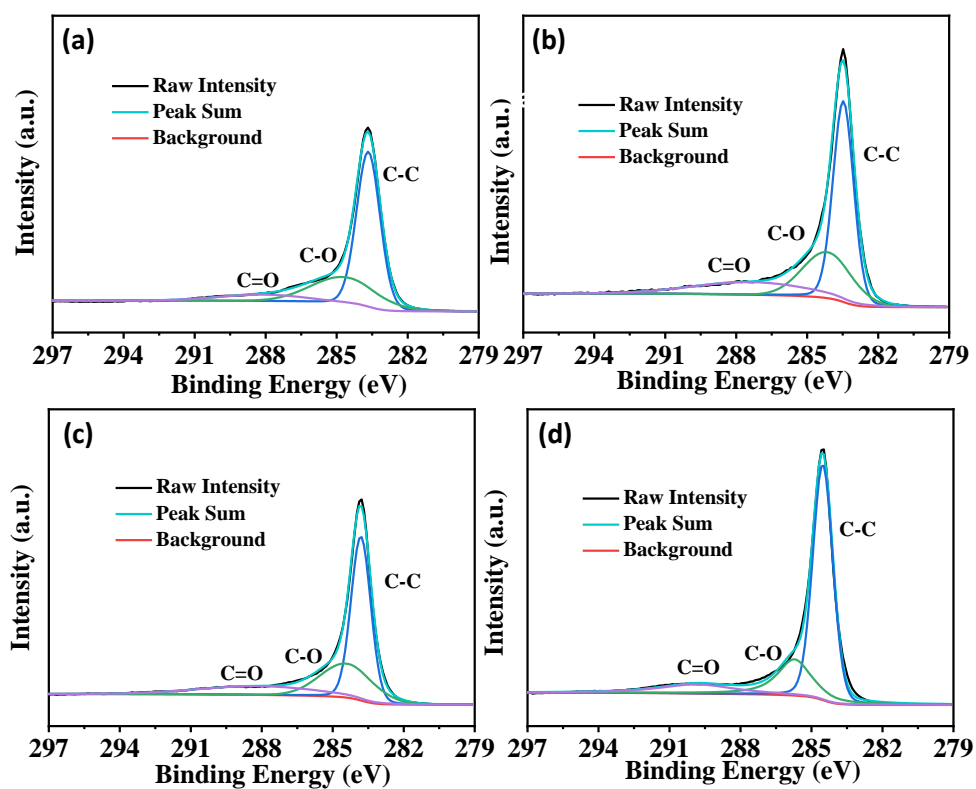


**Fig. S7** Deconvoluted O1s and C1s spectra for samples with different carbonation temperatures: a) HCMB-700, b) HCMB-900, c) HCMB-1100, d) HCMB-1300.

Sample	C-C (eV)/%	C-O (eV)/%	C=O (eV)/%
HCMB-700	283.63/60.22%	284.43/23.7%	286.81/16.08%
HCMB-900	283.47/68.31%	284.75/20.3%	288.09/11.39%
HCMB-1100	283.88/70.8%	284.98/14.96%	288.18/14.24%
HCMB-1300	284.58/77.39%	287.78/11.81%	289.98/10.8%

**Table S2.** Types of chemical bonds, binding energy and the proportion of each bond in the samples at different carbonization temperatures

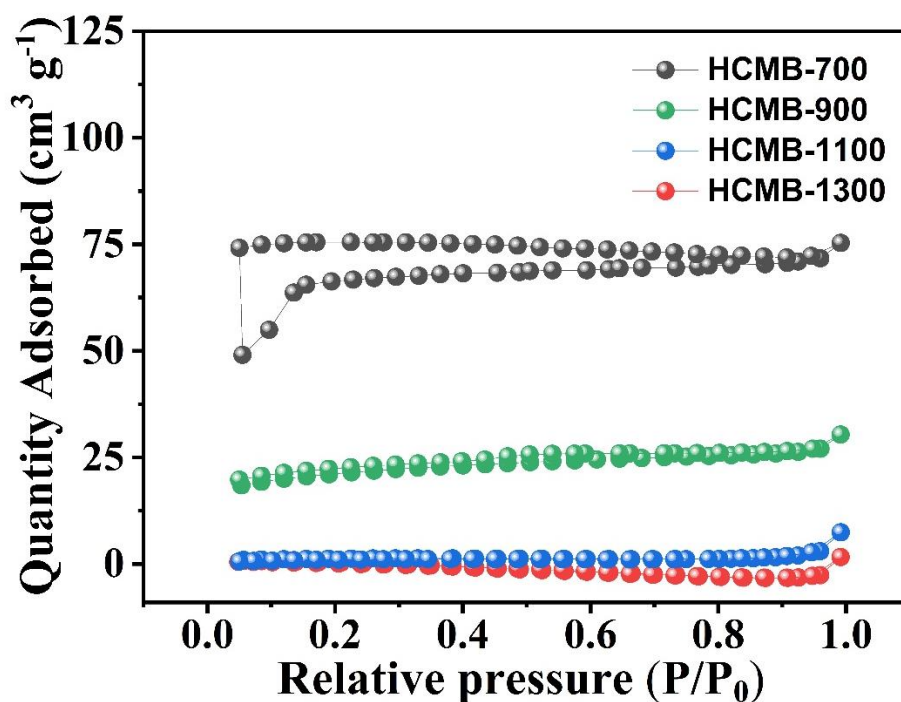


**Fig. S8.** N<sub>2</sub> adsorption/desorption isotherms of HCMB at different carbonization temperatures.

It can be seen that N<sub>2</sub> adsorption/desorption isotherms of HCMB-900, HCMB-1100 and HCMB-1300 could be classified into type II according to the IUPAC classification, indicating the physisorption of N<sub>2</sub> gases on the nonporous surface. HCMB-700 exhibits type I(a) isotherms (see **Fig. S8**), which are given mainly by small micropores on the carbon surface. The surface area is continuously decreased with elevated temperatures from 700 to 1300 °C. Specifically, HCMB-700 has a higher BET surface area (216 m<sup>2</sup> g<sup>-1</sup>) than that of HCMB-900 (68 m<sup>2</sup> g<sup>-1</sup>), HCMB-1100 (4.5 m<sup>2</sup> g<sup>-1</sup>) and HCMB-1300 (0.48 m<sup>2</sup> g<sup>-1</sup>). These results suggest that micropores on the surface of HCMB-700 are open for N<sub>2</sub> molecules, and the pores are gradually closed at over 700 °C and completely closed at 1300 °C, which is in agreement with TEM observation. The closed nanovoids in HCMB-1300 will decrease the irreversible capacity, thus resulting in a high initial Coulombic efficiency (ICE).

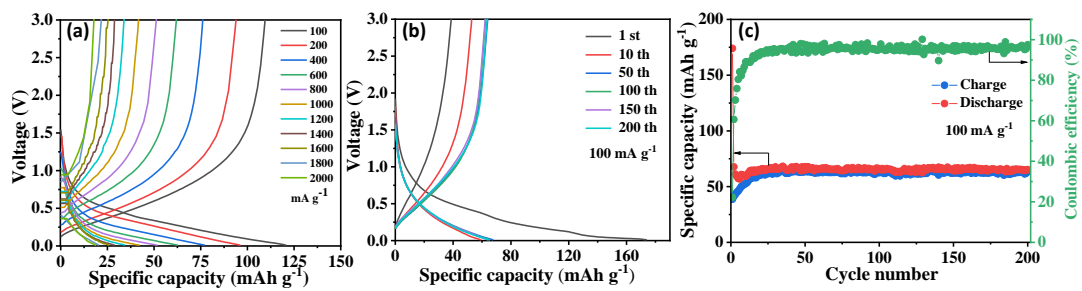


**Fig. S9 Potassium-storage properties in half-cells of HCMB-700.** (a) GCD curves at different current densities, (b) GCD curves at 100  $\text{mA g}^{-1}$ , (c) cycling stability at 100  $\text{mA g}^{-1}$ .

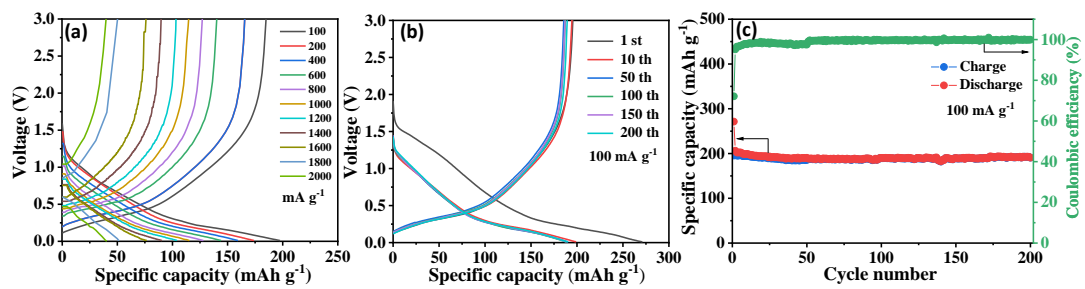


**Fig. S10 Potassium-storage properties in half-cells of HCMB-900.** (a) GCD curves at different current densities, (b) GCD curves at 100 mA g<sup>-1</sup>, (c) cycling stability at 100 mA g<sup>-1</sup>.

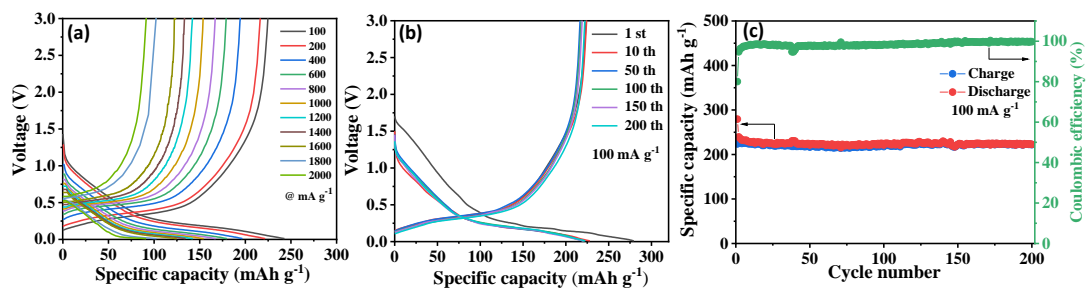


**Fig. S11 Potassium-storage properties in half-cells of HCMB-1100.** (a) GCD curves at different current densities, (b) GCD curves at 100 mA g<sup>-1</sup>, (c) cycling stability at 100 mA g<sup>-1</sup>.

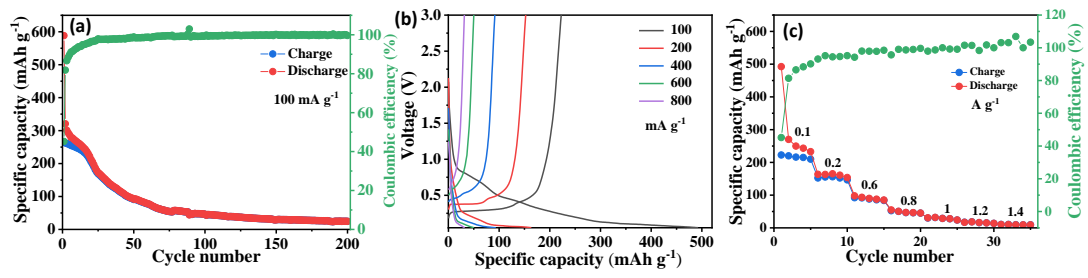


**Fig. S12 Potassium-storage properties in half-cells of graphite.** (a) cycling stability at 100 mA g<sup>-1</sup>, (b) GCD curves at different current densities, (c) rate capability.

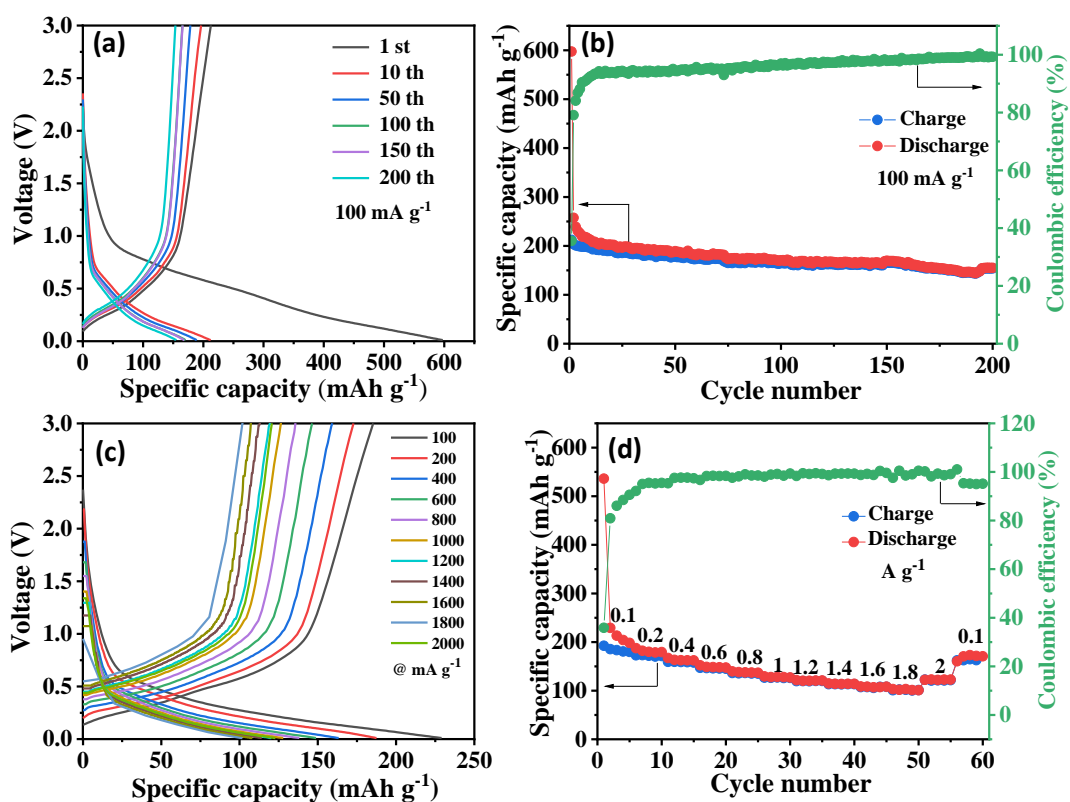


**Fig. S13 Potassium-storage properties in half-cells of pitch.** (a) GCD curves at 100 mA g<sup>-1</sup>, (b) cycling stability at 100 mA g<sup>-1</sup>, (c) GCD curves at different current densities, (d) rate capability.

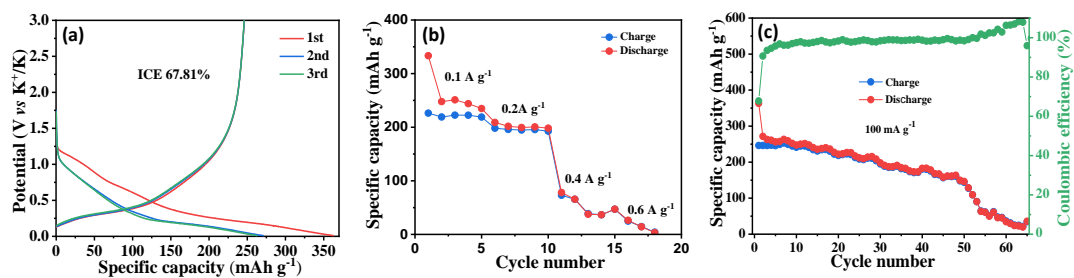


**Fig. S14.** Potassium-storage properties of commercial hard carbon in half-cells: (a) GCD curves at 0.1 A g<sup>-1</sup>, (b) rate capability and (c) cycling performance.

The potassium storage performance of commercial hard carbon (under the same mass loading with HCMB-1300) is shown in **Fig. S14**. It can be clearly observed that the commercial HC electrode exhibits significantly low rate capability and poor cycling performance as compared to HCMB-1300.

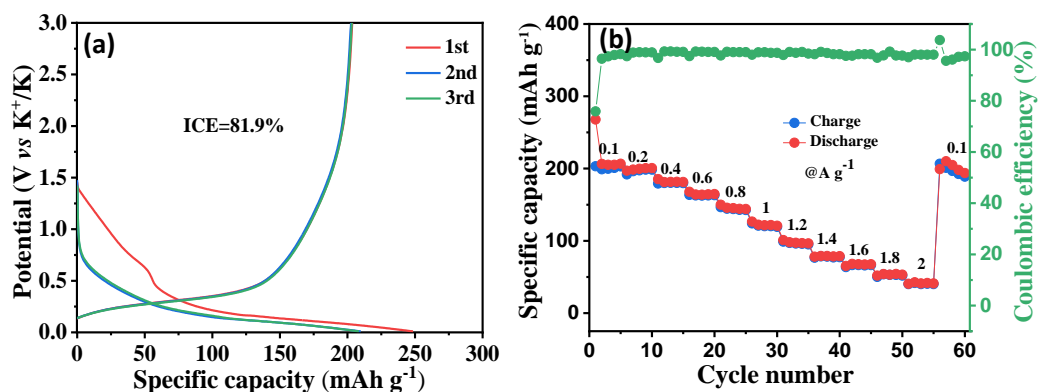


**Fig. S15.** Potassium-storage properties of HCMB-1300 without pre-oxidation: (a) GCD curves at 0.1 A g<sup>-1</sup> and (b) rate capability.

The potassium-storage performance of HCMB-1300 without pre-oxidation is shown in new **Fig. S15**. It can be seen that the HCMB-1300 without pre-oxidation exhibits lower specific capacity (203 mA h g<sup>-1</sup> at 100 mA g<sup>-1</sup>) and inferior rate capability (39 mA h g<sup>-1</sup> at 2000 mA g<sup>-1</sup>) as compared to the HCMB-1300 with pre-oxidation, further demonstrating the importance of pre-oxidation.

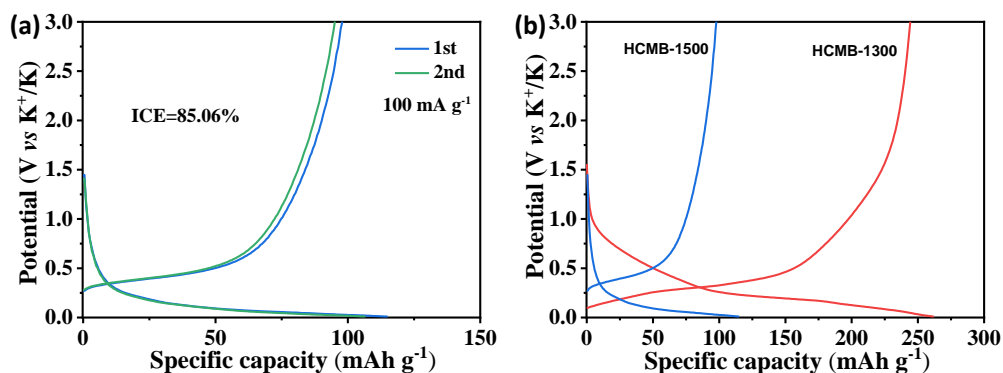


**Fig. S16.** (a) GCD curves of HCMB-1500 at 0.1 A g<sup>-1</sup>, (b) GCD curves of HCMB-1300 and HCMB-1500 at 0.1 A g<sup>-1</sup>.

In order to investigate the effect of high temperature above 1300 °C in the second carbonization process on the battery performance, the pre-oxidized paper was treated at 1500 °C to synthesize the HCMB-1500 sample. The potassium-storage performance of HCMB-1500 is shown in new **Fig. S16**. It can be seen that the ICE value of HCMB-1500 is measured to be 85%, very close to that of HCMB-1300 (88%). The discharge plateau of HCMB-1500 is lower than that of HCMB-1300. However, the potassium-storage capacity of HCMB-1500 is only 115 mA h g<sup>-1</sup> at 100 mA g<sup>-1</sup>, which is much smaller than that of HCMB-1300 (265 mA h g<sup>-1</sup> at 100 mA g<sup>-1</sup>). This result indicates that the higher carbonation temperature (such as 1500 °C) will result in less active K storage sites to correspondingly generate lower specific capacity.

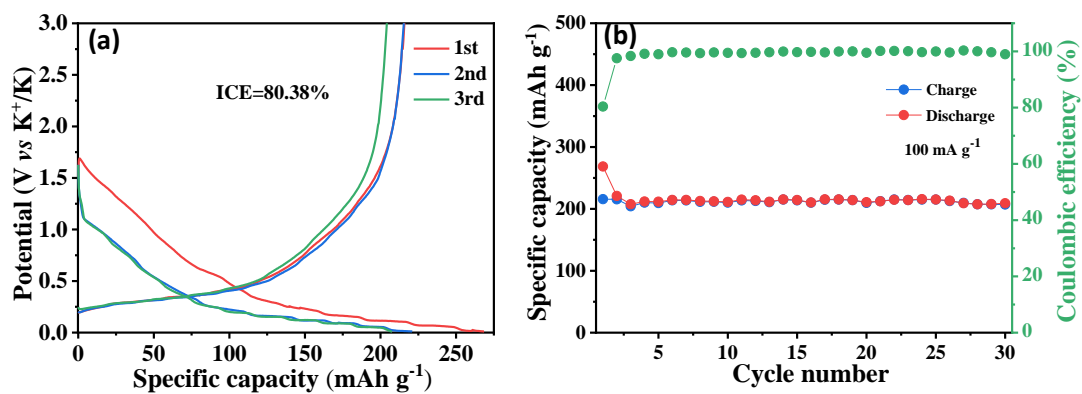


**Fig. S17.** Electrochemical performance of HCMB-1300 at  $0.1 \text{ A g}^{-1}$  in the ether electrolyte (1 M KTFSI in diethylene glycol dimethyl ether). (a) GCD curves, (b) cycling performance.

We measure the potassium storage performance of HCMB-1300 with the ether electrolyte of 1 M KTFSI in diethylene glycol dimethyl ether and the results are shown in new **Fig. S17**. The GCD curves are almost the same in the ether and ester electrolytes. In the ether electrolyte, the ICE value is 83.2%, and the revisable specific capacity is  $214 \text{ mAh g}^{-1}$  at  $100 \text{ mA g}^{-1}$ , which are slightly lower than that in the ester electrolyte (ICE=88.01%,  $265 \text{ mAh g}^{-1}$  at  $100 \text{ mA g}^{-1}$ ). The above analysis has been added in the revised manuscript.

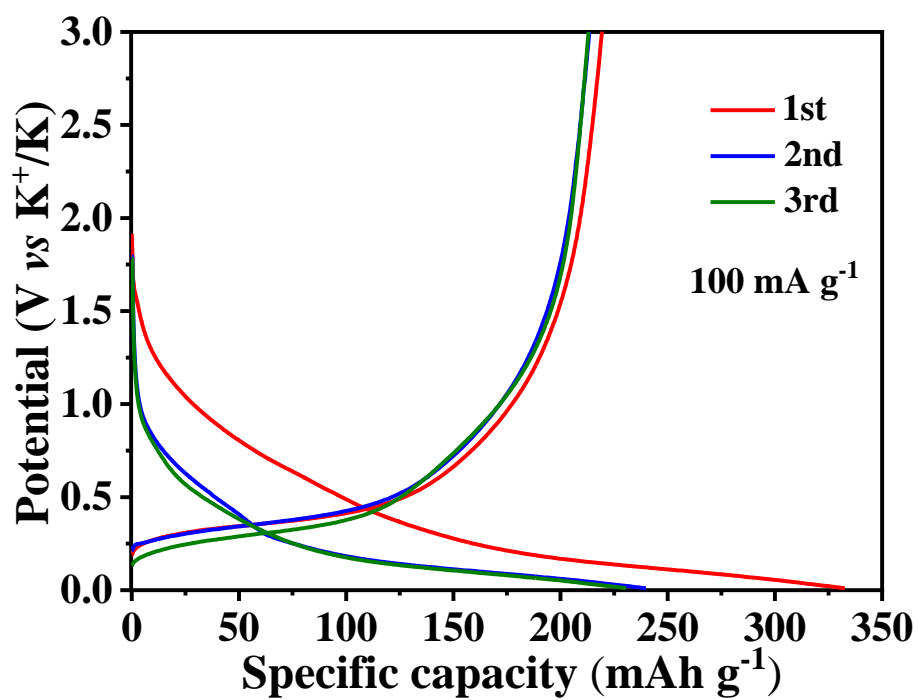


**Fig. S18** GCD curves of the HCMB-1300 powder electrode at 100 mA g<sup>-1</sup>, which was obtained through the traditional slurry-coating technique.

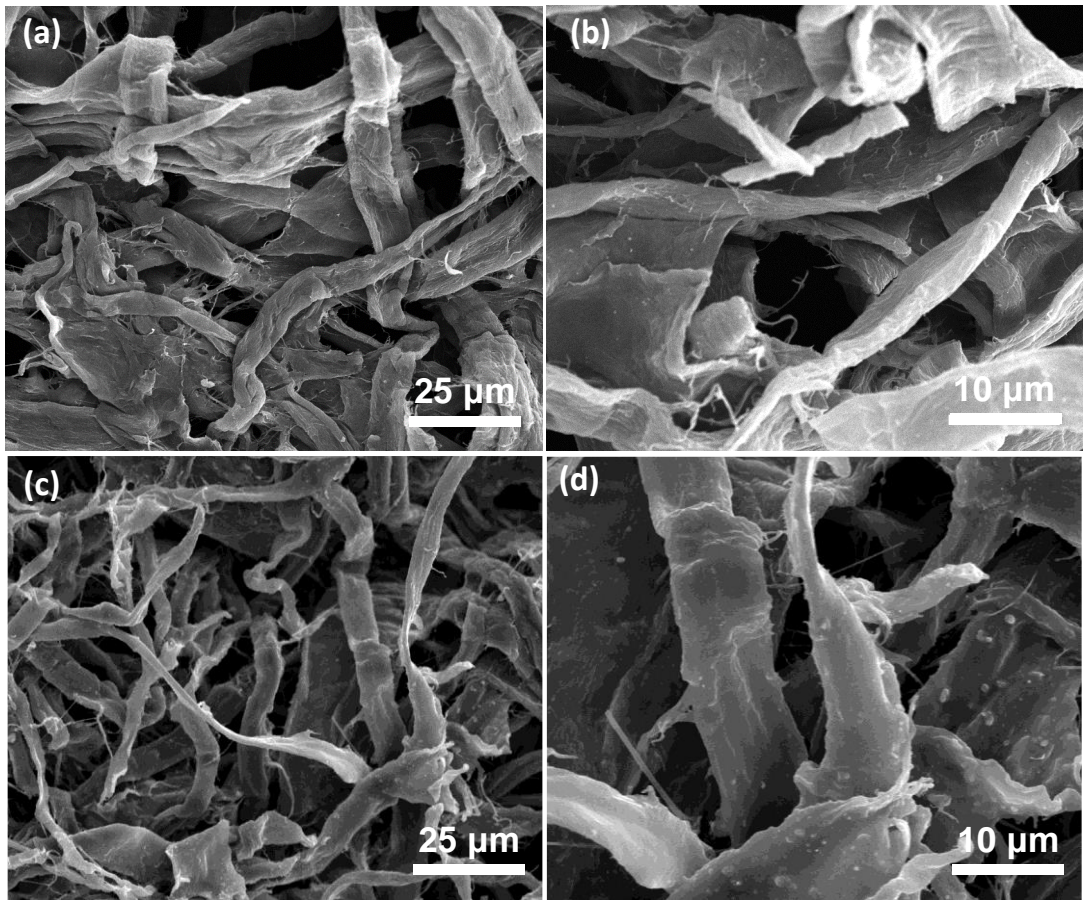


**Fig. S19** SEM images of HCMB-1300 before and after cycling. (a, b) before cycling, (c, d) after cycling.

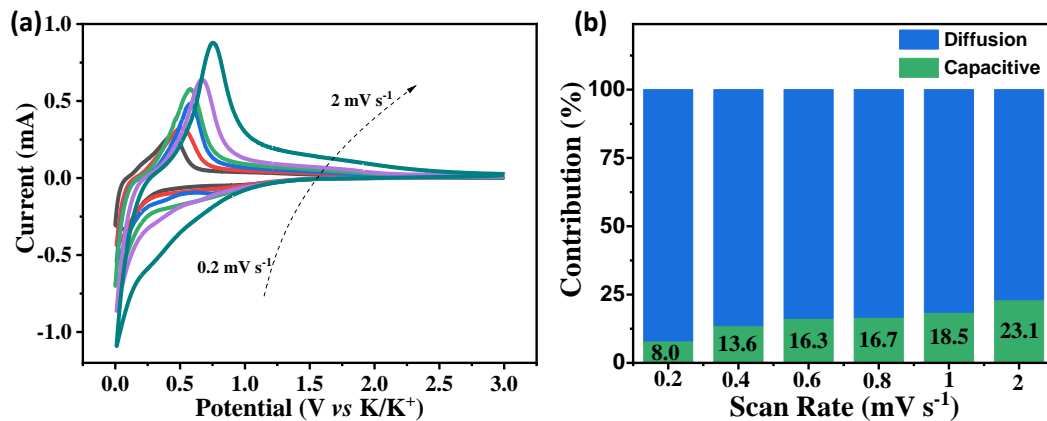


**Fig. S20** (a) CV curves of HCMB-1300 at different scan rates, (b) calculated capacitive contribution of HCMB-1300 at different scan rates.

The capacitive contribution can be quantified by fitting the CV curves using the equations:  $i = k_1v + k_2v^{1/2}$ , where  $k_1v$  represents the contribution from the surface capacitive effect and  $k_2v^{1/2}$  stands for diffusion-controlled reaction. By plotting  $v^{1/2}$  vs.  $i/v^{1/2}$ ,  $k_1$  and  $k_2$  can be obtained through the slope and the intercept point in y-axis, respectively. As we can see (**Fig. S20b**), the capacitive contribution is as low as 23.1% even at  $1 \text{ mV s}^{-1}$ . This result indicates that the potassium-storage kinetics could mainly be diffusion-controlled.

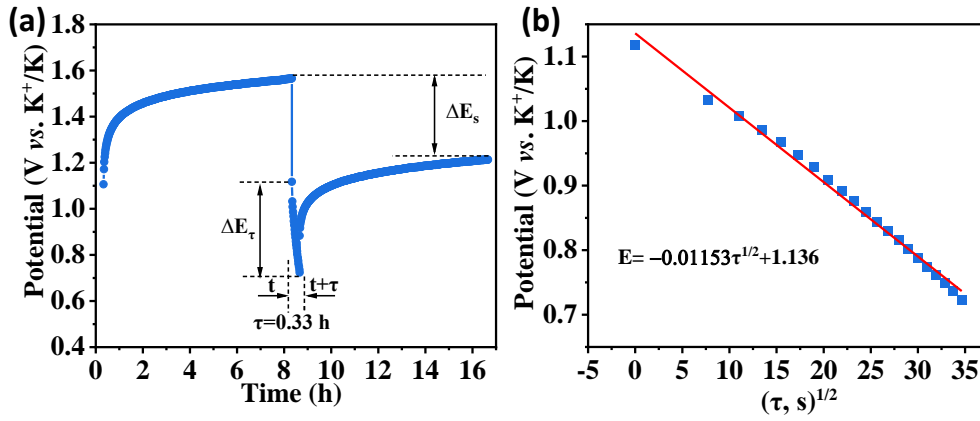


**Fig. S21** Schematic diagram of a single-step titration during GITT measurement, the voltage profile before, during and after a constant current pulse with schematic labeling of different parameters.

GITT is an effective method for determining the chemical diffusion coefficient in mixed electron and ion conductors. Assuming that  $K^+$  transport in the electrode obeys Fick's second law, since  $E_t$  and  $\tau^{1/2}$  follow a linear relationship, as shown in Figure S15b, the apparent  $K^+$  chemical diffusion coefficient ( $D_{K^+}$ ) in the single-phase region can be calculated by:

$$D_{K^+} = \frac{4}{\pi\tau} \left( \frac{m_B V_M}{M_B S} \right)^2 \left( \frac{\Delta E_S}{\Delta E_\tau} \right)^2 \quad (\tau \ll L^2/D) \quad [1]$$

where  $m_B$  is the mass of the active material in the electrode,  $V_M$  is the molar volume,  $M_B$  is the molecular weight of the material,  $S$  is the active surface area between the electrolyte and the electrode,  $\Delta E_S$  is the difference in the steady-state voltage of the cell, and  $\Delta E_\tau$  is the total transient voltage difference of the cell for the time  $\tau$  of the applied current.  $\tau$  is the length of time of applied current and  $L$  is the diffusion distance of  $K^+$  from the lattice to the liquid electrolyte, so the equation [1] can be further simplified to [2].

$$D_{K^+} = \frac{4}{\pi\tau} \left( \frac{R_S}{3} \right)^2 \left( \frac{\Delta E_S}{\Delta E_\tau} \right)^2 \quad [2]$$

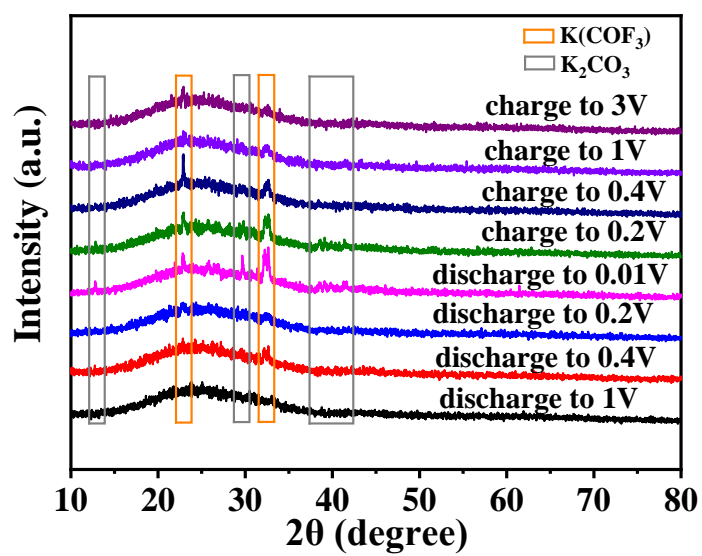


**Fig. S22** The ex situ XRD patterns of HCMB-1300 at different discharge–charge states at  $0.1 \text{ A g}^{-1}$ .

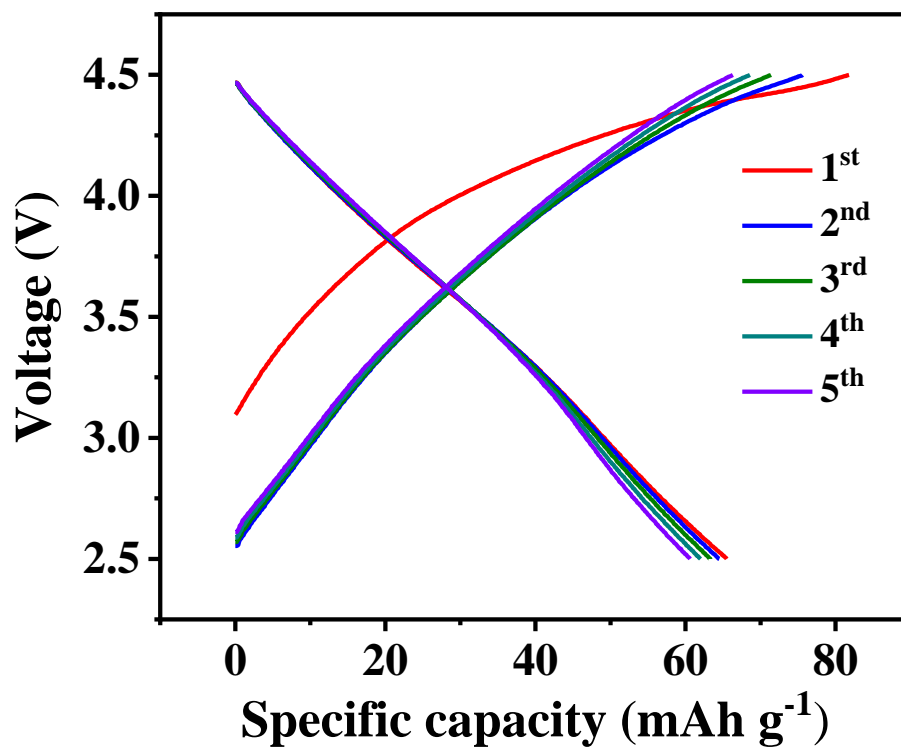
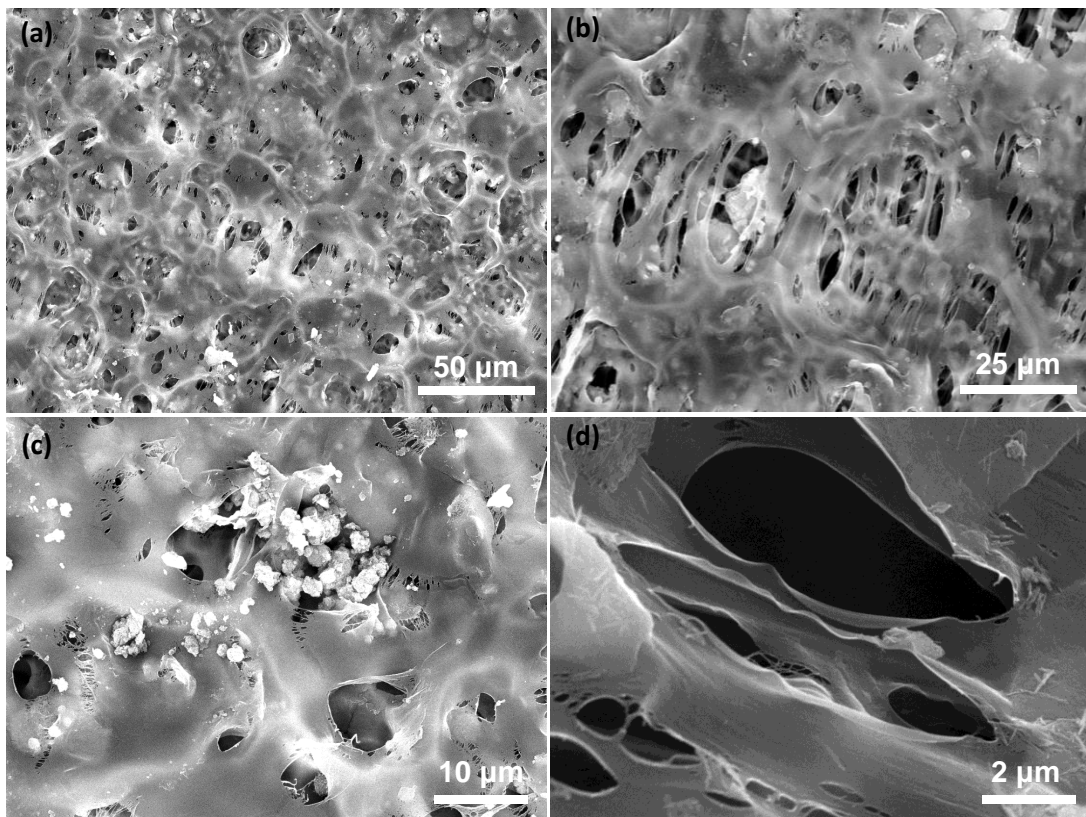


Fig. S23 Electrochemical performance of the AC cathode at 0.1 A g<sup>-1</sup> in half-cells.



**Fig. S24** SEM of the gel electrolyte sepiolite/PVDF-(HFP).